International Journal of Heat and Mass Transfer 52 (2009) 2624–2631

Contents lists available at ScienceDirect

International Journal of Heat and Mass Transfer

journal homepage: www.elsevier.com/locate/ijhmt

Single-phase heat transfer, friction, and fouling characteristics of three-dimensional cone roughness in tube flow

Ralph L. Webb *

Department of Mechanical and Nuclear Engineering, The Pennsylvania State University, University Park, PA 16802, United States

ARTICLE INFO

Article history:
Received 13 July 2008
Available online 9 March 2009

Keywords:
Roughness
Single phase
Enhanced
Heat transfer
Fouling
Three-dimensional
Helical-rib

ABSTRACT

This paper reports heat transfer and friction characteristics of three tubes having a conical, three-dimensional roughness on the inner tube surface with water flow in the tube. The TC3 truncated cone tube has twice the cone area density as TC2 and provides a Nusselt number 3.74 times that of a plain tube. The h-value is 36% higher than TC2, but it has it has nearly 60% higher pressure drop. The three-dimensional roughness offers potential for considerably higher heat transfer enhancement (e.g., 50% higher) than is given by helical ridged tubes, such as the Turbo-B type. The two truncated cone tubes provide 14–20% higher h-value than the commercial Wolverine Turbo BIII tube. Further, they have both have approximately 5% higher efficiency index than Turbo BIII. Accelerated particular fouling data are also provided for 3-D tube TC3, and for helical-ribbed tubes. The results show that although the 3-D tube provided the highest heat transfer coefficient, relative to a plain tube (h/h_p), it also had the highest asymptotic fouling resistance, relative to a plain tube (R_f^+/R_p^+). Significant long-term fouling would not be expected in applications using relatively clean water.

1. Introduction

Internally enhanced tubes for liquid flow are very important in commercial applications. The refrigeration industry routinely uses roughness on the water-side of large refrigeration evaporators and condensers, as described by Webb [1] and Webb and Kim [2]. Such evaporators and condensers have water flow inside the tubes with evaporation (or condensation) on the outside of tubes in a bundle. If a plain inner tube surface is used, the controlling thermal resistance will be on the tube (water) side. Use of internal enhancement considerably reduces the tube-side thermal resistance. An example of a commercially available tube is shown in Fig. 1, is the 19 mm O.D. "helically ribbed" Turbo BII tube having 38 internal starts, which was introduced by Wolverine in 1995. A recent patent by Thors et al. [3] describes commercial versions of helically ribbed tubes developed by Wolverine. Several manufacturers make a tube similar to Fig. 1. Recent papers reporting data on "helically ribbed" tubes are by Webb et al. [4], and Zdaniuk et al. [5,6]. Fig. 2 illustrates the "rolling method" used to make a tube having internal and external enhancements. This method uses a grooved internal mandrel, and typically three sets of external dies located at 120 degree intervals around the tube circumference.

A variety of internally enhanced geometries have evolved since the mid-1970s. These tubes are described in Chapter 9 of Webb and Kim [2]. Some work has also been done on three-dimensional tube-side enhancement. Such enhancements are shown in Figs. 9.18 and 9.19 of Webb and Kim [2]. Performance data from Webb and Kim [2] are compared in Table 1 for a variety of tube geometries for water (Pr = 10.4) at $Re_d = 25{,}000$. Table 1 also lists the internal enhancement dimensions. The tubes are listed in order of increasing h/h_p. The greatest heat transfer enhancement is provided by the Turbo BIII^J and the 3-D roughness Tred-19D^J tube. The pressure drop of the Tred-19D^J tube appears to be lower than is expected. Although the 3-D roughness tube A8 reported by Takahashi [7] is not a commercial geometry, it is included in Table 1 for comparison. It provides even higher performance than Turbo BIII^J or the Tred-19D^J tube. The A8 tube provides 3.75 times higher heat transfer coefficient and 3.35 times higher friction than a plain tube. This enhancement is made by two internal mandrels. The first mandrel makes internal fins at one helix angle. The second mandrel makes internal fins at an opposite helix angle. When the second mandrel cuts across the first set of fins, a three-dimensional pyramidal roughness is formed. Their tubes (A-3, A-6, and A-8) the second forging process penetrated the full rib height, resulting in 3-D roughness of a pyramidal in shape (trapezoidal in cross-section), that are oriented at an angle to the primary flow direction.

Tube-side fouling is a concern in such tubes that provide high heat transfer enhancement. Accelerated particulate fouling tests on five of the tubes reported by Webb et al. [4] were conducted using 3.0 μm aluminum oxide particles. The particulate fouling data were taken on Tubes 2, 3, 4, 5, and 8 shown in Fig. 1 of Li and Webb [8] and a plain tube.

* Tel.: +1 814 235 7358.
E-mail address: Ralph.Webb@psu.edu

0017-9310/$ - see front matter © 2009 Elsevier Ltd. All rights reserved.
doi:10.1016/j.ijheatmasstransfer.2009.01.008

Nomenclature

A	inside surface area based on nominal diameter ($\pi D_i L$), m^2
B	time constant in Kern–Seaton (1959) fouling equation, 1/s
$B(e^+)$	friction correlating function for rough tubes $[(2/f)^{½} + 2.5\ln(e/D_i) + 3.75]$, dimensionless
D_i	internal tube diameter, or diameter to root of fins, m
e	Rib height (average value), m
e^+	roughness Reynolds number ($= eu^*/v$), dimensionless
$\bar{g}(e^+)$	heat transfer correlating function, $[f/(2St) - 1]/(f/2)^{1/2} + B(e^+)]\mathrm{Pr}^{-n}$, dimensionless
f	Fanning friction factor, dimensionless
G	mass velocity, kg/m^2 s
h	heat transfer coefficient based on $A = \pi D_i L$, W/m^2 K
K_m	mass transfer coefficient based on $A = \pi D_i L$, kg/m^2 s
Nu	Nusselt number ($= hD_i/k$), dimensionless
p_t	transverse rib pitch, viewed normal to the ribs ($= \pi D_i/N_s$), m
p_l	axial rib pitch [$(= p_n/\tan\alpha)$], m
Pr	Prandtl number, dimensionless
Re	tube-side Reynolds number ($= D_i G/\mu$), dimensionless
Sc	Schmidt number
u^*	Friction velocity $[= (\tau_w/\rho)^{1/2}]$, m/s

Greek letters

α	helix angle, degrees
η	efficiency index, $(h/h_p)/(f/f_p)$, dimensionless
ϕ_d	rate of foulant deposition, m^2 K/W s
ϕ_r	rate of foulant removal, m^2 K/W s
v	kinematic viscosity, m^2/s
μ	dynamic viscosity at bulk water temperature, kg/m s
μ_w	dynamic viscosity at wall temperature, kg/m s
ρ	fluid density, kg/m^3
τ_w	wall shear stress, Pa

Subscripts

i	internal surface
p	plain surface
c	clean
f	fouled

Superscripts

*	asymptotic value

This paper provides original data on a new three-dimensional tube developed by the author. The performance of this tube is among the best shown in Table 1. Accelerated particulate fouling data were also taken on this tube for 1300 ppm foulant concentration at 1.07 m/s water velocity (Re = 16,000). The fouling rate is compared with helical-rib geometries reported by Li and Webb [8].

2. Three-dimensional enhancement geometry

Tubes having three-dimensional inside enhancement was designed for manufacture using a method of roller embossing flat copper strip between embossed circular rollers having small cone shaped depressions. A pattern of conical holes was formed in the circular shaped cylinder tool using the electrostatic discharge machining (EDM) process. Once the cone shapes were embossed on the copper strip, the strip was then rolled into a circular shape and seam welded. Three variants of the 3-D roughness were made for testing. The dimensions of these enhancements are given in Table 2. Fig. 3 shows the cone pattern described in Table 2. The transverse pitch of the cones in all three TC tubes is the same (3.10 mm). The TC1 and TC2 tubes have 3.10 mm axial pitch, while the TC3 tube has half the axial cone pitch as the TC1 and TC2 tubes (1.55 mm). Thus, TC3 has twice the cone area density as tubes TC1 and TC2. A principal difference difference in the tubes is the cone height, as defined in Table 3. A photo of the TC3 tube is shown in Fig. 4. Detailed performance data are provided here for tube TC3. Limited performance data are provided to compare tubes TC2 and TC1 with tube TC3.

3. Experimental apparatus and calibration

Heat transfer data were taken in the double-tube test section shown in Fig. 5 by running city water in the annulus and re-circulating water in the tube side. The cold city water in the annulus cooled the warm re-circulating water inside the test section. The instrumentation consists of a differential pressure transducer, pressure taps at the inlet and exit of the tube, four thermistors (two at the tube inlet and outlet, and two at the annulus inlet and outlet), two flow meters, a centrifugal pump, and a water tank. Steady state was achieved by heating the re-circulating water by an electric heater. The heat balance between the two fluid streams was always within 5.5%. For all the data points, the heat load calculated from the tube side was slightly higher than the annulus side.

The smooth surface and the enhanced I.D. tubes are connected using a small piece of rubber hose at each end. The two surfaces were pushed into the pieces of hose until they touched, then the rubber pieces were tightened by metal straps to prevent any water leakage. The two ends of copper tubing attached to the hose were de-burred and had the same inside diameter. The water was heated to 22 °C

Fig. 1. Photos of Wolverine Turbo BII™ tube.

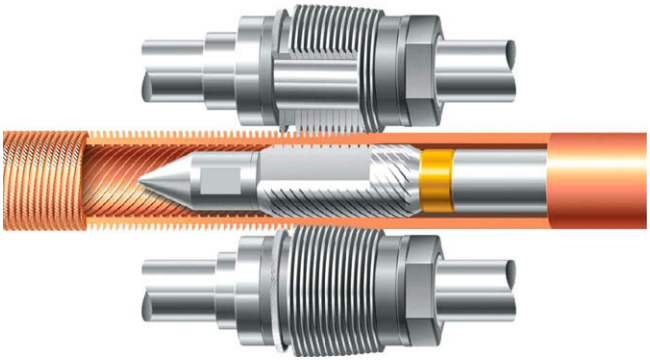

Fig. 2. Method of making internal/external finned tube.

Table 1
Performance comparison of commercial enhanced tubes from Webb and Kim [2] (d_o = 19.05 mm, Re = 25,000, Pr = 10.4).

Tube	d_i (mm)	e/d_i	n_s	p/e	α (degree)	h/h_p	f/f_p	η
GEWA-TW[J]	15.3	0.016	1	5.3	89	1.40	1.40	1.00
Thermoexcel-CC™	14.97	0.025	1	46.7	73	1.59	1.90	0.84
GEWA-SC™	15.02	0.035	25	2.67	30	1.87	1.65	1.13
Korodense™ (LPD)	17.63	0.025	1	20.3	81	1.89	2.26	0.84
Turbo-Chil	14.60	0.026	10	11.1	47	1.98	1.83	1.08
Korodense (MHT)	17.63	0.04	1	12.0	81	2.50	4.63	0.54
Tred-26d™	14.45	0.024	10	7.63	45	2.24	1.88	1.19
Turbo-B™	16.05	0.028	30	1.94	35	2.34	2.14	1.09
Turbo BIII LPD	16.38	0.022	34	3.56	49	2.40	1.98	1.21
Turbo BIII	16.38	0.025	34	3.22	49	2.54	2.30	1.10
Tred-19D™	14.45	0.024	10	7.63	57	2.55	1.76	1.45(?)
A8 (Table 9.8)	13.5	0.036	2	7.6	30	3.75	3.35	1.11
TC3	17.32	0.024	–	1.68	–	3.74	4.38	0.85

Table 2
Truncated cones tubes (19.05 mm O.D., 17.32 mm I.D.).

Tube geometry	Cone height e (mm)	Cone transverse pitch p_t (mm)	Cones axial pitch p_l (mm)	Cone base diameter d_o (mm)	e/D_i	p_t/e	p_l/e
TC1	0.51	3.10	3.10	0.79	0.029	6.08	6.08
TC2	0.38	3.10	3.10	0.79	0.022	8.16	8.16
TC3	0.43	3.10	1.70	0.79	0.025	7.21	3.95

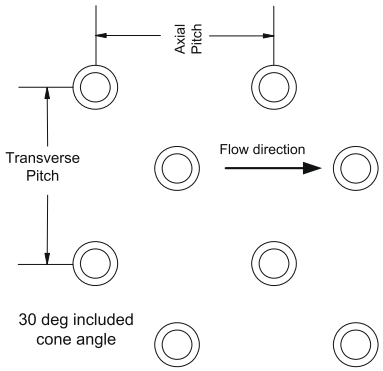

Fig. 3. Geometric definition of axial pitch and transverse pitch.

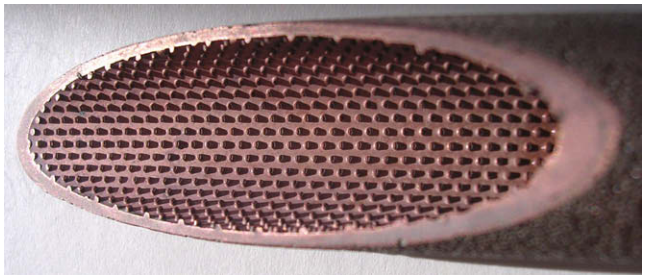

Fig. 4. Photo of enhancement of TC3 tube.

Table 3
Measured Nusselt numbers for Praxair data at Re = 24,000.

Test	Nu	Pr	Nu_{adj} (at Pr = 6.4)
1	619.5	9.235	506.3
2	668.8	9.220	547.1
3	573.3	9.018	474.8

before taking data. The temperature was monitored by measuring the inlet water temperature to maintain steady temperature throughout the experiment. The brass annulus tube was 25.4 mm O.D. and 22.1 mm I.D. The 22.1 mm inside diameter provided a reasonable resistance ratio between the tube and annulus flows.

4. Test results

Two independent tests on the Fig. 4, 3-D roughness geometry were performed at Penn State University and at Praxair Corp. These tests and the results are described below.

4.1. Penn State data

The pressure drop data were taken for adiabatic water flow. Fig. 6 shows the friction factor vs. Reynolds number for the tube TC3, and the Blasius equation for a smooth tube ($f_p = 0.079Re^{-1/4}$). At Re = 10,000, $f/f_p = 3.75$, where f_p is the plain tube value.

The modified Wilson plot method as described by Farrell et al. [9] was used to determine the annulus water-side heat transfer coefficient. Then, a power-law expression for the annulus side Nusselt number was developed. The expression has the form

$$Nu_D = C\,Re^m\,Pr^{1/3} \quad (1)$$

The annulus side heat transfer coefficient was held constant by keeping the annulus water flow rate and average water temperature in the annulus constant. The data were taken at a tube side Reynolds number range of 4000–24,000 and the Prandtl number varied from 6.6 to 5.9. A valid Wilson plot requires that the Reynolds number exponent be constant over the test range. Hence, the data for 4000–9000 Reynolds number transition regime are not included in the Wilson plot correlation. Fig. 7 shows the resulting Wilson plot calibration using the data with high Reynolds numbers, 9000–24,000. The thermal resistance on the inside of the tube for the Wilson plot data varied from 31% to 54% of the total thermal resistance.

The heat transfer characteristics of the apparatus was evaluated by first testing a 15.9 mm O.D. plain tube. The experimental data were compared to existing heat transfer correlations (Petukhov and Sieder-Tate) as found in Incropera and DeWitt [10]. The measured heat transfer data agreed almost precisely with the Petukhov equation and was about 5% higher than for the Sieder-Tate equation with a leading coefficient of 0.027.

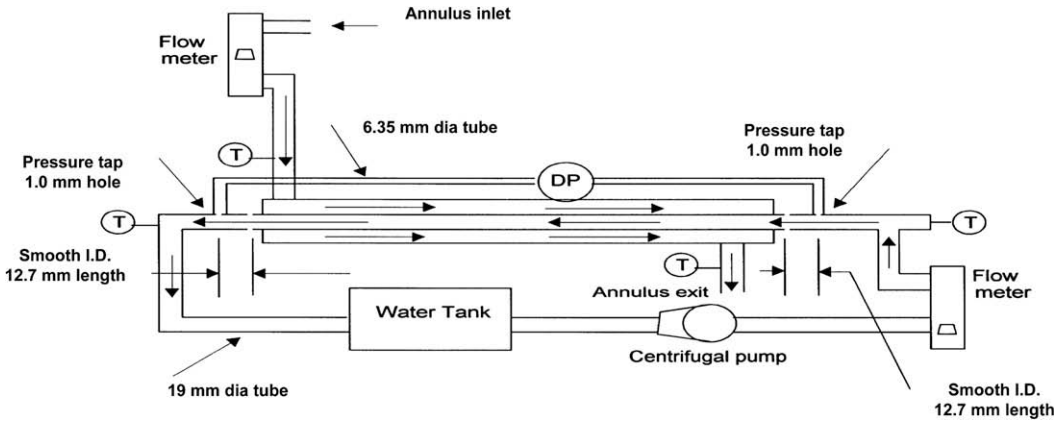

Fig. 5. Schematic of clean tube test apparatus.

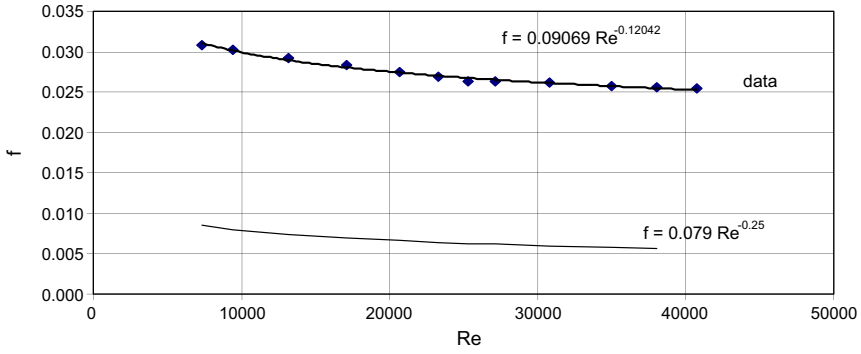

Fig. 6. Friction factor vs. Reynolds number for the tube TC3.

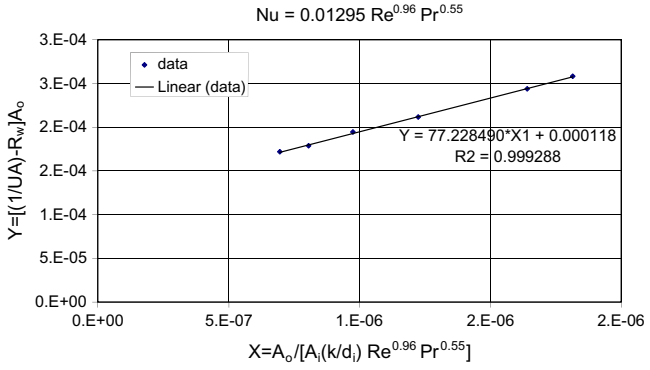

Fig. 7. Wilson plot line for the tube TC3.

The resulting correlation for the tube-side Nusselt number for the truncated cone geometry is shown on Fig. 8 and is given by

$$\mathrm{Nu} = 0.01295\mathrm{Re}^{0.96}\mathrm{Pr}^{0.55} \quad (9000 < \mathrm{Re} < 24,000) \tag{2}$$

Evaluation of the derived tube-side coefficient suggests that the Reynolds number exponent is not constant in the 4000–9000 Reynolds number range. This can be seen by inspection of Fig. 8, which shows the derived Nu vs. Re curve for the tube-side heat transfer coefficient. Fig. 8 is prepared for Pr = 6.4.

The small variation of Prandtl number (5.9–6.6) in the Wilson plot calibration was accounted for using the correction $\mathrm{Nu}\,\mathrm{Pr}^{0.55}$. This is recommended in by Webb and Kim [2] and is based on tests of a variety of rough surfaces. It was further validated by Brognaux et al. [11] for tests of microfin tubes with single-phase heat transfer.

The experimental uncertainty was determined using the method of Kline and McLintock [16] and is presented in Appendix A.

4.2. Praxair test results

An independent test was run on the truncated cone tube by Ragi [12] at the Praxair research lab in Tonawanda, NY. Their friction tests showed $3.6 < f/f_p < 4.2$ for $20,000 < \mathrm{Re} < 50,000$, as compared to the present data values of $3.6 < f/f_p < 4.5$ for $7000 < \mathrm{Re} < 41,000$. These values are considered in reasonable agreement.

Praxair performed three separate tests for heat transfer data of the truncated cone tube, which were taken at Pr = 9.24–9.02. Their heat transfer tests were performed on a tube having the "High-Flux" boiling surface coating on the outer surface. The tests were performed by boiling a fluid on the outer tube surface and cooling water inside the tube. The boiling coefficient (h_{nb}) was assumed to be known as a function of saturation temperature and heat flux, based on previous tests done on separate boiling surfaces. Thus, the equation was used to calculate the boiling was of the form $h_{nb} = \mathrm{const} \times (q/A)^n$, where const and n are empirical terms determined in the separate boiling tests. The boiling side thermal resistance was subtracted from the overall resistance to obtain the tube-side thermal resistance. The average heat flux over the full tube length was used to evaluate h_{nb}. This was calculated from the water flow rate and water temperature change. Dr. Ragi stated that the water-side resistance was controlling in the UOP tests.

Ragi [12] performed three separate tests for heat transfer data of the truncated cone tube, which were taken at Pr = 9.24–9.02, as compared to the Penn State tests at Pr = 6.4. The derived water-side heat transfer coefficients were curve-fitted as a function of Reynolds number. The Praxair curve fit values of the Nusselt number at

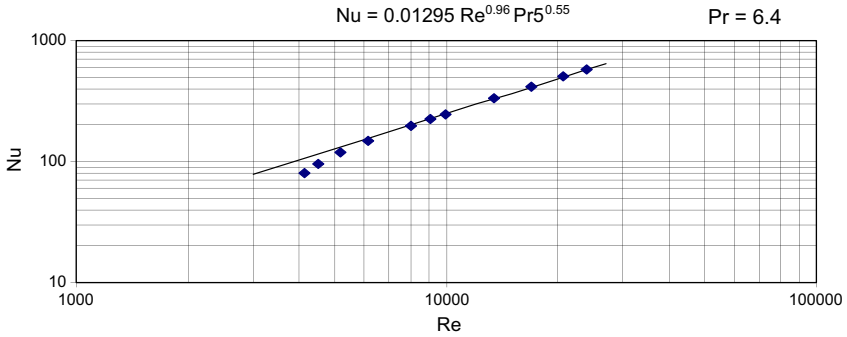

Fig. 8. Nusselt number vs. Reynolds number for the tube TC3.

Re = 24,000 for their three tests is shown in Table 3. Webb and Kim [2] and Brognaux et al. [11] have shown that Nu% $Pr^{0.55}$ for rough tubes. Using the correction $Nu_{adj} = Nu\,(6.4/Pr)^{0.55}$, the Ragi [12] data at Re = 24,000 were adjusted to Pr = 6.4, which resulted in the Nusselt values 506.3, 547.1, and 474.8 as shown in Table 3. The arithmetical average of these three corrected Nusselt values is 509.4. The Penn State data taken at Pr = 6.4, showed Nusselt value of 576.3 for Re = 24,000. Hence, the adjusted Praxair Nusselt number (509.4) is 12% smaller than the present test result (576.3). Using only the two higher values of the corrected Nu for the Praxair data (506.3 and 547.1) yields a Nu value 9% smaller than the Penn State value. Thus, we conclude that the Penn State test results are 9–12% above the Praxair test values. This comparison of two independent test results serves as good confirmation of the Penn State test results.

5. Prandtl number dependency

Data were taken at Penn State on tube TC2 to define the Prandtl number dependency. These data were taken with water at three temperatures (giving Pr = 3.5, 6.8, and 8.2) plus air (Pr = 0.71). The Prandtl number dependency is determined in the form of the heat-momentum analogy for rough surfaces as described in Section 9.3.3 of Webb and Kim [2]. This method allows one to plot the data in the form

$$\bar{g}(e^+)\mathrm{Pr}^n = \frac{f/(2St) - 1}{\sqrt{f/2}} + B(e^+) \tag{3}$$

where $B(e^+)$ is the "friction similarity" parameter determined from pressure drop tests. This term is defined by Eq. (9.10) of Webb and Kim [2]. The friction data yielded

$$B(e^+) = 4.76(e^+)^{0.10} \tag{4}$$

where e^+ is the "roughness Reynolds number" defined as eu^*/ν.

A cross-plot of the data in the form of Eq. (3) for different Prandtl numbers allows determination of the exponent "n" on the Prandtl number. Finally, the data for TC2 were plotted in the form $\bar{g}(e^+)\mathrm{Pr}^{-0.44}$ vs. e^+. This resulted in the correlation,

$$\bar{g}(e^+) = 6.74(\mathrm{e}+)^{0.19}\mathrm{Pr}^{0.44} \tag{5}$$

which one may use with Eqs. (3) and (4) to predict the heat transfer coefficient for other dimensionless cone heights (e/D_i) and Prandtl numbers. Note that the surface geometry must be maintained geometrically similar. This means that one must maintain a fixed element shape, and a constant ratio for the roughness dimensions p_t/e, p_l/e, and d_c/e. So, if the roughness height (e) is reduced 25%, the dimensions p_t, p_l, and d_c must also be reduced by 25%.

6. Discussion of results

Table 4 compares the performance of the truncated cone tubes (TC1, TC2, and TC3) with the Wolverine Turbo BIII tube at Re = 27,000 and Pr = 9.35, which is close to the Re = 25,000, Pr = 10.4 values of Table 1. Table 4 shows the friction factor ratio (f/f_p), the Nusselt number ratio (Nu/Nu_p) and the "efficiency index," defined as $\eta = (h/h_p)/(f/f_p)$. The truncated cone values are calculated by using curve-fits of the Penn State data. The plain tube Nusselt values (Nu_p) are calculated using the Petukhov correlation and the plain tube friction factors (f_p) are calculated using Filonenko friction correlation given in Incropera and DeWitt [10]. The Turbo BIII data are taken from Webb et al. [4], whose source is the Wolverine patent on Turbo BIII as given in Thors et al. [3].

As seen in Table 4, the Turbo BIII tube provides approximately 2.3 times increase in heat transfer and friction factor, which gives an efficiency index of 0.99. The TC3 truncated cone tube has an 88% higher Nu/Nu_p than the Turbo BIII tube. However, the TC3 "efficiency index" is 14% smaller than the Turbo BIII tube. The other two truncated cone tubes have nearly equal performance and provide 14–20% higher Nusselt number than for Turbo BIII. Further, they have both have approximately 5% higher efficiency index than Turbo BIII. Note that the 33% higher cone height of TC1 yields 8.3% higher h-value and 4.5% friction factor than for the TC2 tube. Hence, both the TC1 and TC2 tubes are clearly superior to Turbo BIII.

The performance of the truncated cone tubes were also compared with Turbo BIII using the FN-2 performance comparison from Table 3.1 of Webb and Kim [2]. The FN-2 evaluation assumes all of the thermal resistance is on the tube side, maintains fixed flow rate, flow velocity, and heat transfer rate, and compares the required heat transfer surface area and pumping power. The Turbo BIII tube is used as the reference tube. The results are shown in Table 5. The TC1 tube provides 23% reduced surface area and 7% reduction of pumping power. The truncated TC2 tube provides 16% reduced surface area and 4% reduction of pumping power. The TC3 tube allows 38% reduced heat transfer area, but requires 16% more pumping power. If the fluid velocity were reduced by using more tubes in parallel, the pumping power would be reduced.

The heat transfer enhancement (h/h_p) of the TC3 tube is approximately equal to that of the Takahashi (1988) three-dimensional A8 tube. However, the reported f/f_p of the A8 tube is approximately 23% less than for the TC3 tube. It is possible that further optimization of the TC3 and A8 tube types are possible. This may be done

Table 4
Comparison of heat transfer enhancement and friction factor increase for Turbo BIII with the truncated cone tubes (Re = 27,000 and Pr = 9.35).

Tube	f/f_p	Nu/Nu_p	η
Turbo BIII	2.33	2.31	0.99
TC1	2.78	2.98	1.07
TC2	2.66	2.75	1.04
TC3	4.38	3.74	0.85

Table 5
FN-2 performance comparison of truncated cone tubes against Turbo BIII.

Tube	$f/f_{\text{Turbo BIII}}$	$\text{Nu}/\text{Nu}_{\text{Turbo BIII}}$	$A/A_{\text{Turbo BIII}}$	$P/P_{\text{Turbo BIII}}$
TC1	1.29	1.20	0.77	0.93
TC2	1.19	1.14	0.84	0.96
TC3	1.62	1.88	0.62	1.16

using the heat-momentum transfer analogy correlation of Eq. (3) to predict the performance for a geometrically similar tube having a smaller e/D_i ratio. The author has used Eq. (3) with Eqs. (4) and (5) to predict the heat transfer coefficient and pressure drop for different values of e/D_i. This analysis shows that for $e/D_i = 0.01$ and Re = 25,000, the friction factor for is 20% lower than that for $e/D_i = 0.022$. In addition, the Stanton number for $e/D = 0.0l$ is only 2% lower than for $e/D_i = 0.022$. Therefore, the analysis shows that if we keep p_t/e, p_l/e, and d_c/e constant and reduce e/D to 0.010, the heat transfer coefficient drops only 2%, while the friction factor is reduced by 20%, relative to the TC3 tube. Such a tube geometry is recommended for further development.

7. Accelerated fouling tests

Because the TC3 tube gives such a high enhancement level, it is of interest to define its fouling performance. Accelerated particulate fouling tests were conducted to investigate the effects of the internal surface geometry on the fouling behavior of the TC3 tube listed in Table 2. This work an extension of the particulate fouling data taken in Tubes 2, 3, 4, 5, and 8 of Li and Webb [8]. The foulant material is 3.0 μm diameter aluminum oxide particles suspended in water. These tests were performed for 1300 ppm foulant concentration and at 1.07 m/s water velocity (Re = 16,000).

The tests were conducted in the apparatus described by Webb and Kim [13]. Because the apparatus and test procedure were described by Webb and Kim, only brief description will be given here. The apparatus has three fouling test sections, with one being a plain tube. Heat is transferred to the 3.05 m long test sections by condensing R-114 on the annulus side of the test section. Condensed R-114 is returned to the electric-heated boilers. Each test section has its own boiler, in which R-114 is heated by three electric band heaters (each of 1200 W capacity). Power to the band heaters surrounding the R-114 tanks is controlled by individual auto-transformers and the heat is removed from the test water in a plate heat exchanger. The fouling resistance is obtained by taking the difference between the overall thermal resistances for the fouled condition ($1/U_f$) and the clean tube condition ($1/U_c$). The data for U_f and U_c are taken at the same velocity, heat flux and water inlet temperature. The clean tube data were taken using clean water.

The apparatus was run for two hours with clean water to reach a steady state. After it reached a steady state, the amount of particulate required for the desired ppm concentration was added to the system. This was taken as time zero for the next fouling test series, which was approximately 18 h.

Data for the particulate laden water were taken with 1.07 m/s water velocity for 1300 ppm ± 10% foulant concentration. After the foulant was added, no additional foulant was added during the test period. This was done to prevent instabilities that could affect the fouling rate, or the retention of the foulant deposit. For 1300 ppm initial concentration, the foulant concentration decreased approximately 200 ppm during the test.

Fouling is a rate-dependent phenomenon. The net fouling rate is the difference between the particle deposition rate and the removal rate. Kern and Seaton [14] proposed an asymptotic fouling model that is applicable to particulate fouling. They expressed the net fouling rate as the difference between the deposition and the removal rate:

$$\frac{dR_f}{dt} = \phi_d - \phi_r \tag{6}$$

where dR_f/dt = net fouling rate, ϕ_d = deposition rate, and ϕ_r = removal rate.

7.1. Fouling and heat transfer relationship

The foulant deposition rate (ϕ_d) should be proportional to the mass transfer coefficient (K_m) obtained from the heat-mass transfer analogy. The mass transfer coefficient (K_m) is given by the heat-mass transfer analogy,

$$\frac{K_m}{u_m}\text{Sc}^{2/3} = \frac{h}{\rho u_m c_p}\text{Pr}^{2/3} \tag{7}$$

Eq. (7) shows that a high clean tube heat transfer coefficient should result in a high mass transfer coefficient. Hence, enhanced heat transfer surfaces (regardless of what kind of enhancement) should result in higher foulant deposition rates than occur with plain surfaces at the same operating velocity.

The key requirement to use the heat-mass transfer analogy is that the mass transport occur within the diffusion region. For particles less than about 10 μm, the particle transport will be diffusion controlled. In the diffusion regime, particles move with the fluid, and are carried to the wall through the viscous sublayer by Brownian motion. The submicron particles can then be treated as large molecules, and K_m can be predicted via turbulent heat transfer data (or correlations) via the heat-mass transfer analogy.

7.2. Fouling test results

Fig. 9 shows the accelerated particulate fouling curves for 1300 ppm concentration particulate fouling data at 1.07 m/s and 16,000 Reynolds number. It shows that the enhanced tubes exhibit higher fouling resistance than the plain tube. In addition, the fouling rate attains an asymptotic value for all the tubes. The greatest fouling increase occurred in the three-dimensional TC3 tube and the helical-rib tubes 2, 3, and 5.

Table 6 shows the asymptotic enhanced-to-plain tube fouling ratio (R_f^*/R_p^*), which includes the helical-rib data from Li and Webb [8]. Table 6 also shows the ratio of the enhanced-to-plain tube heat transfer coefficients (h/h_p), where h_p is the clean tube data. The clean tube data are reported and discussed by Webb et al. [4]. It

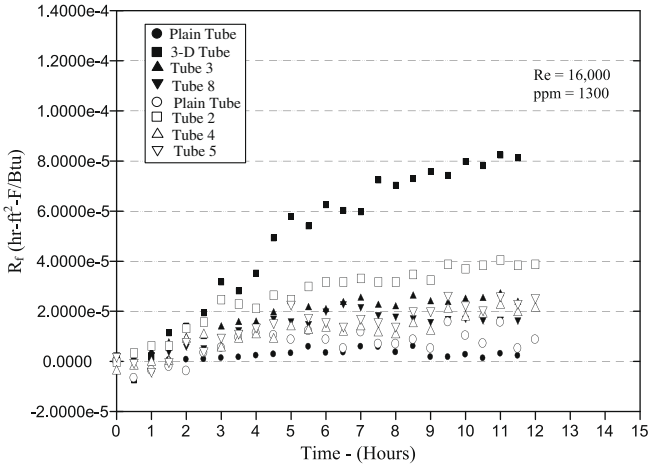

Fig. 9. Accelerated particulate fouling data of helical-ribbed and 3-D tubes taken at 1.07 m/s water velocity.

Table 6
Ratio of asymptotic fouling resistance and ratio of heat transfer coefficient of enhanced tubes, both relative to the plain tube (accelerated fouling were not taken for tubes 6 and 7).

Tube	3-D	2	5	3	6	7	8	4	Plain tube
R_f^*/R_p^*	15.28	7.28	5.28	3.28	n/a	n/a	2.00	2.57	1.0
h/h_p	2.7	2.32	2.26	2.33	2.08	1.93	1.55	1.74	1.0

is interesting to compare the R_f^*/R_p^* ratios (enhanced-to-plain tube) with the h/h_p ratios. The h/h_p ratios vary from 1.55 to 2.33. Table 6 shows that the three-dimensional TC3 tube has the highest h/h_p ratio. It also has the highest R_f^*/R_p^*. The next highest R_f^*/R_p^* is shown by helical-ribbed tube 2. The Table 3 data suggests a strong link between R_f^*/R_p^* and h/h_p.

Although the foulant deposition rate is proportional to K_m, and K_m %h, we cannot conclude that high K_m will necessarily result in a high R_f^*. It is also necessary to consider the effect of the enhancement geometry on the foulant removal process (ϕ_r), which is proportional to the wall shear stress (τ_w). The Kern and Seaton [14] model shows that the $R_f^* \propto K_m/\tau_w$. The surface shear stress (τ_w) is not directly proportional to pressure drop in helically ribbed tubes, because of pressure drag caused by flow separation. A geometry that provides high K_m and a small wall shear stress will be a candidate for high R_f^* – as is the case for the small p_a/e, high helix angle tubes (tubes 2, 3, and 5), which all have small p_a/e (resulting in low velocity recirculation zones in the axial zone between ribs) and large helix angle (causing higher pressure drag) than for the other helically ribbed tubes. Hence, it is probable that they will have smaller τ_w than for the tubes having a smaller number of starts, or smaller helix angles. It is probable that the small p_a/e of Tube 2 causes small τ_w and is responsible for its high R_f^*. Fig. 9 suggests that significant fouling will occur in helical-rib tubes when $p_a/e < 4.0$.

7.3. Effect of internal surface geometry

Li and Webb [8] developed an empirical correlation of their helical-rib geometry fouling data to define the effect of the geometric variables using the functional groups geometric groups rib pitch-to-height (p/e), dimensional roughness height (e/D_i), and helix angle (α). The result is

$$R_f^* \propto (p/e)^{-0.994}(e/D_i)^{0.00032}\alpha^{0.000241} \quad (8)$$

Eq. (8) shows that the dominant parameter affecting fouling in the helical-rib tubes is the helical-rib pitch-to-height (p/e) geometric variable. Eq. (8) shows that the effect of e/D_i and α on R_f^* are very small. The flow pattern in the wall region the 3-D roughness geometry is significantly different from that of the helical-ribbed tubes geometry. It is probable that flow separation effects will be smaller than for the small p/e helical-rib tubes.

Although the 3-D tube showed a higher fouling rate than the helical-ribbed tubes, one should not conclude that high fouling will occur in all applications. For example, the tube should experience minimal and acceptable low fouling, if used with relatively clean or treated water, as is used in large water chiller systems. Such results were found in fouling tests of different internally enhanced geometries and reported by Haider et al. [15].

8. Conclusions

1. The two truncated cone tubes (TC1 and TC2) have nearly equal performance and provide 14–20% higher h-value than the Turbo BIII. Further, they have both have approximately 5% higher efficiency index than Turbo BIII.
2. The TC3 truncated cone tube has twice the cone area density as TC2 and provides $Nu/Nu_p = 3.74$ (36% higher h-value than TC2), but it has it has nearly 60% higher pressure drop.
3. Use of a 3-D roughness offers potential for considerably higher heat transfer enhancement (e.g., 50% higher) than is given by helical-rib tubes, such as the Turbo B type. However, optimization work remains to be done to select the e/D_i ratio that gives high efficiency index at the desired operational Reynolds number.
4. Based on the use of Eq. (4), a tube geometrically similar to TC3 with $e/D_i = 0.01$ will have 20% lower friction factor and 2% lower Stanton number than for the tested TC3 tube.
5. The 3-D roughness tube TC3 shows a very high accelerated particulate fouling rate, which is higher than that of the helical-ribbed tubes tested by Webb and Li (1999).
6. The 3-D roughness tube should experience minimal and acceptable low fouling, if used with relatively clean or treated water, as occurs in water chiller flooded evaporators.

Acknowledgments

The research done in this work was sponsored by Olin Brass Corp., who made the 3-D roughness tubes. The author also acknowledge contributions made by Dr. Louay Chamra, Mustafa Yanik, and Ram Narayanamurthy in the clean tube tests of the 3-D roughened tube. Dr. Wei Li performed the fouling tests.

Appendix A. Experimental uncertainty

The experimental uncertainty for the clean tube heat transfer and friction measurement was determined using the method of Kline and McLintock [16]. The uncertainty associated with the highest error in component is given in Table A.1. The error is assumed to be zero for the density and diameter.

Using the uncertainty analysis, the uncertainty in friction factor is given by

$$\frac{\Delta f}{f} = \sqrt{\left(\frac{\Delta L}{L}\right)^2 + \left(\frac{\Delta(\Delta P)}{(\Delta P)}\right)^2 + 2\left(\frac{\Delta \dot{V}}{\dot{V}}\right)^2} \quad (A.1)$$

The measured maximum uncertainty in the friction factor is 5.96% for a flow rate of 2.8 l/min. For a flow rate of 7.6 l/min, the error decreases to 1.8%.

A similar procedure is applied for heat transfer. For heat transfer, the data reduction equation can be written as

$$\frac{1}{h_i} = \frac{\Delta T_{lm}}{Q_{av}}A_i - R_w A_i - \frac{1}{h_o}\frac{A_i}{A_o} \quad (A.2)$$

The uncertainty in the log-mean temperature difference is 1.4%. The corresponding error in the heat flux is calculated to be 3.6%. The error in calculation of the total resistance is 3.9%. The error for each point of the Wilson plot will be a function of the x- and y-axis of the Wilson plot. The error in the Wilson plot was calculated to be 5%. Hence, the error in computation of h_o will be equal to 5%.

Table A.1
Instrumental uncertainties.

Instrument	Accuracy	Maximum uncertainty (%)
Thermistor	0.0055 C	0.5
Pressure transducer	0.25% of calibrated span	1.6
Turbine flowmeter	0.1% of full scale	4
Rotameter	0.38 l/min	3.3
Tube length	2.0 mm	0.1

The error in calculation of h_i will be a function of the percentage of resistances on the inside and outside. At the extreme condition the resistance on the inside is no less than 35% of the total resistance. In that case, with both errors the uncertainty of the inside resistance in terms of the total resistance would be 7%. This would mean that the uncertainty of the inside heat transfer coefficient, $\Delta h_i/h_i$, would be 20%. This is an extreme condition and statistically using a root mean square value, the uncertainty would be evaluated to be 5% of the total resistance, i.e., 14%. For most data points, the inside resistance is greater than 60%, for which the uncertainty would be 8%.

References

[1] R.L. Webb, Advances in shell side boiling of refrigerants, J. Inst. Refrig. 87 (1991) 75–86.
[2] R.L. Webb, N.-H. Kim, Principles of Enhanced Heat Transfer, second ed., Taylor & Francis, New York, 2005 (Chapter 9).
[3] P. Thors, N.R. Clevinger, B.J. Campbell, J.T. Tyler, Heat Transfer Tubes and Methods of Fabrication thereof, U.S. Patent No. 5,697,430, 1997, assigned to Wolverine Tube.
[4] R.L. Webb, R. Narayanamurthy, P. Thors, Heat transfer and friction characteristics of internal helical-rib roughness, J. Heat Transfer 122 (2000) 134–142.
[5] G.J. Zdaniuk, L.M. Chamra, D. Keith Walters, Correlating heat transfer and friction in helically-finned tubes using artificial neural networks, Int. J. Heat Mass Transfer 50 (23–24) (2007) 4713–4723.
[6] G.J. Zdaniuk, L.M. Chamra, P.J. Mago, Experimental determination of heat transfer and friction in helically-finned tubes, Exp. Therm. Fluid Sci. 32 (3) (2008) 761–775.
[7] K. Takahashi, W. Nakayama, H. Kuwahara, Enhancement of forced convective heat transfer in tubes having three-dimensional spiral ribs, Heat Transfer Jpn. Res. 17 (4) (1988) 12–28.
[8] W. Li, R.L. Webb, Fouling in enhanced tubes using cooling tower water. Part II: Combined particulate and precipitation fouling, Int. J. Heat Mass Transfer 43 (2000) 3579–3588.
[9] P. Farrell, K. Wert, R.L. Webb, Heat transfer and friction characteristics of turbulent radiator tubes, SAE Trans. 99 (1991) 737–750. Section 5.
[10] F.P. Incropera, D.P. DeWitt, Fundamentals of Heat and Mass Transfer, fifth ed., John Wiley & Sons, New York, 2001 (Chapter 8).
[11] L. Brognaux, R.L. Webb, L.M. Chamra, B.K. Chung, Single-phase heat transfer in micro-fin tubes, Int. J. Heat Mass Transfer 40 (1997) 4345–4358.
[12] E. Ragi, Private communication with Praxair Corp, 1999.
[13] R.L. Webb, N.-H. Kim, Particulate fouling in tubes having a two-dimensional roughness geometry, Int. J. Heat Mass Transfer 34 (1991) 2727–2738.
[14] D.Q. Kern, R.E. Seaton, A theoretical analysis of thermal surface fouling, Br. Chem. Eng. 14 (3) (1959) 258–262.
[15] S.I. Haider, R.L. Webb, A. Meitz, Tube-side fouling in water-chiller flooded evaporators, ASHRAE J. 35 (10) (1993) 59–67.
[16] S.J. Kline, F.A. McClintock, Describing uncertainties in single-sample experiments, Mech. Eng. 75 (1953) 3–8.